

1 **Structural study of the C-terminal domain of non-structural protein 1 from**
2 **Japanese encephalitis virus**

3

4 Thanalai Poonsiri^{a,c}, Gareth S. A. Wright^a, Michael S. Diamond^d, Lance Turtle^{b, c}, Tom
5 Solomon^c, Svetlana V. Antonyuk^{a#}

6

7 ^aMolecular Biophysics Group, Institute of Integrative Biology, Faculty of Health and Life
8 Sciences, University of Liverpool, UK, ^bCentre for Global Vaccine Research and ^cHealth
9 Protection Research Unit on Emerging and Zoonotic Infections, Institute of Infection and
10 Global Health, University of Liverpool, Liverpool, UK. ^dDepartments of Medicine,
11 Molecular Microbiology, Pathology & Immunology, Washington University in St. Louis,
12 St. Louis, USA

13

14 Running Head: Structure of NS1 from Japanese encephalitis virus

15

16 #Address correspondence to Dr. Svetlana V Antonyuk, S.Antonyuk@liverpool.ac.uk.

17

18 **Abstract**

19 Japanese encephalitis virus (JEV) is a mosquito-transmitted Flavivirus that is
20 closely related to other emerging viral pathogens including dengue, West Nile (WNV)
21 and Zika viruses. JEV infection can result in meningitis and encephalitis, which in
22 severe cases cause permanent brain damage and death. JEV occurs predominantly in
23 rural areas throughout Southeast Asia, the Pacific islands and the Far East, causing
24 around 68,000 cases worldwide each year. In this study, we present a 2.1 Å resolution
25 crystal structure of the C-terminal β -ladder domain of JEV non-structural protein 1 (NS1-
26 C). The surface charge distribution of JEV NS1-C is similar to WNV and ZIKV but differs
27 from DENV. Analysis of the JEV NS1-C structure, with *in silico* molecular dynamics
28 simulation and experimental solution small angle X-ray scattering, indicates extensive
29 loop flexibility on the exterior of the protein. This, together with the surface charge
30 distribution, indicates flexibility influences the protein-protein interactions that govern
31 pathogenicity. These factors also affect the interaction of NS1 with the monoclonal
32 antibody, 22NS1, which is protective against West Nile virus infection. Liposome and
33 heparin binding assays indicate that only the N-terminal region of NS1 mediates
34 interaction with membranes, and that sulfate binding sites common to NS1 structures
35 are not glycosaminoglycan binding interfaces. This study highlights several differences
36 between flavivirus NS1 proteins and contributes to our understanding of their structure-
37 pathogenic function relationships.

38 **Importance**

39 JEV is a major cause of viral encephalitis in Asia. Despite extensive vaccination,
40 epidemics still occur. Non-structural protein 1 (NS1) plays a role in viral replication and,
41 because it is secreted, it can exhibit a wide range of interactions with host proteins. NS1
42 sequence and protein folds are conserved within the Flavivirus genus, but variations in
43 NS1 protein-protein interactions among viruses likely contribute to differences in
44 pathogenesis. Here, we compared characteristics of the the C-terminal β -ladder domain
45 of NS1 between flaviviruses including surface charge, loop flexibility, epitope cross-
46 reactivity, membrane adherence, and glycosaminoglycan binding. These structural
47 features are central to NS1 functionality and may provide insight into the development
48 of diagnostic tests and therapeutics.

49 **Introduction**

50 JEV is a positive-sense single strand RNA virus with a 10.9 kb genome, which is
51 translated into a polyprotein consisting of three structural proteins (capsid, membrane,
52 and envelope protein (E)), and seven non-structural proteins ((NS)1, NS2A, NS2B,
53 NS3, NS4, NS4B, and NS5). Flavivirus NS1 is a multifunctional glycoprotein that has
54 drawn attention because of its importance in viral replication, immune modulation, and
55 immune evasion. Mutagenesis and trans-complementation assays have established
56 that flavivirus NS1 is essential for RNA replication (1-5) and co-localizes with the
57 replication complex (2). Transcomplementation suppressor mutagenesis studies
58 indicate that YFV NS1 interacts with NS4A (6) and WNV NS1 interacts with NS4B (7).
59 WNV NS1 forms a physical complex with NS4B based on coimmunoprecipitation
60 experiments (7). NS1 has been described as a complement fixing antigen (8-11), and
61 DENV NS1 binds to complement pathway components C1s, C4, C4b (12, 13) whereas
62 WNV NS1 also can interact with factor H (14) to which protect infected cells from
63 complement-dependent clearance. NS1 also may interfere with the dsRNA sensor Toll-
64 like receptor 3 (TLR-3) (15) to escape host pathogen recognition receptor detection.
65 DENV NS1 can induce inflammatory cytokine production, endothelial cell permeability,
66 and changes to the glycocalyx (16) possibly through interactions with TLR-4, all of
67 which appear to contribute to the development of severe dengue (17, 18). Although
68 direct interactions between JEV NS1 and TLR-4 have not been evaluated, it may play a
69 role in JEV pathogenesis, because deletion of the TLR-4 gene enhances resistance to
70 JEV (19).

71 A signal sequence at the C-terminus of E protein translocates NS1 to the
72 endoplasmic reticulum (ER) where it undergoes cleavage and posttranslational
73 modification (20). There are two characterized forms of NS1: a membrane-associated
74 dimer (~49 kDa per monomer), found on ER surface and the plasma membrane, and a
75 secreted hexamer (52- 55 kDa per monomer) (20). The mass of the two NS1 forms are
76 different due to differential glycosylation. Structures of full-length WNV (21, 22), DENV
77 (22), and ZIKV NS1 (23, 24) proteins have been reported. Most NS1 proteins contain
78 six conserved disulfide bonds. NS1 shares a conserved N-linked glycosylation site at
79 Asn 207. YFV, DENV, WNV, and JEV share a second glycosylation site at Asn 130, and
80 most of the JE serogroup NS1 proteins have a third glycosylation site at Asn175 linked
81 to high-mannose carbohydrate, but this is not present in JEV NS1 itself (20, 25-27).
82 The NS1 monomer of WNV, DENV and ZIKV contains 3 domains: β -roll (amino acid
83 residues 1-29), wing (38-151), and β -ladder domains (181-352) (22-24). NS1 forms a
84 homodimer by extending the β -ladder domain and connecting at β -roll domain forming a
85 cross shape protein. One face of the dimer comprises of the protruding β -roll and part of
86 the wing domain. The hydrophobic surface of the β -roll and wing domains may mediate
87 the interaction with the cell membrane (22) via a number of amino acid residues
88 identified from ZIKV, including 28, 115, 118, 123, and 160-163 (23, 24). The opposite
89 side is composed of loops linking the surface β -strands of the ladder domain. This
90 region is a potential host protein interacting surface due to its hydrophilicity. Three NS1
91 dimers can assemble to form a hexameric pore, which can act as a lipid depot (22, 28).
92 DENV NS1 expression on the infected cell surface may occur via a
93 glycosylphosphatidylinositol (GPI) anchor, for which a hydrophobic carboxy-terminal

94 GPI-addition signal peptide at the N-terminus of NS2A is required (29-31). Soluble NS1
95 also binds to uninfected cell membranes via glycosaminoglycans (GAGs), primarily
96 heparan sulfate and chondroitin sulphate E (32).

97 Secreted NS1 is used as diagnostic marker for flavivirus infection, as it is found
98 in the blood at early stages (33, 34). Alternatively, detection of anti-NS1 IgM and IgG
99 can be used (34, 35). Immunization of NS1 in mice or passive transfer of anti-NS1
100 antibodies can confer protective effects against flavivirus challenge (34, 36-39).
101 However, some anti-DENV NS1 antibodies reportedly are autoreactive and bind to host
102 extracellular matrix components, platelets, and endothelial cells (8, 20), which may have
103 pathogenic consequences. Flavivirus NS1 transferred with blood meal was found to
104 enhance viral infection in mosquitoes by downregulating mosquito midgut immune
105 genes (40).

106 Most of our knowledge of JEV NS1 has been inferred from studies of DENV and
107 WNV NS1. Although the protein sequences are highly conserved (**Fig 1**) and the DENV,
108 WNV, and ZIKV NS1 structures display the same protein fold, there are important
109 differences. For example, polyclonal antibodies raised against DENV NS1 in mice were
110 shown to cross-react with proteins on epithelial cell: ATPase, protein disulfide
111 isomerase, vimentin, and heat shock protein 60. The cross-reactive epitope was
112 mapped to amino acid residues 311-330 on DENV NS1 (41) (**Fig 1**). Although JEV NS1
113 shares these conserved epitopes, antibodies against JEV NS1 did not react to any of
114 these host cell targets (41). NS1 alone was shown to cause endothelial leakage in
115 DENV, but this was not detected in WNV, consistent with the non-vascular leakage
116 phenotype of WNV disease (42). Similar to WNV, other encephalitic flaviviruses

117 including JEV may vary in their NS1-endothelium interactions. As another example,
118 WNV NS1 binds the alternative complement pathway regulator, factor H, whereas JEV
119 NS1 does not (8).

120 NS1' is an extended form of NS1 with 52 extra amino acids from the NS2A N-
121 terminus, generated by a -1 ribosomal frameshift (43). It is specific to the JE serogroup
122 of flaviviruses. NS1' was found in dimeric form (monomer molecular mass around 58
123 kDa), detected in both cell lysate and culture media (44, 45), and suggested to play a
124 role in neuroinvasiveness; selectively abolishing NS1' production reduces WNV
125 mortality in mice (43, 46). NS1' co-localized with viral RNA replication complex, and can
126 substitute for NS1 in cells (45). However, there is a discrepancy between the results of
127 *in vitro* and *in vivo* studies. WNV NS1' provides an advantage only in *in vivo* studies
128 (47). There is also variation of NS1' involvement in replication among different viruses.
129 Whereas WNV NS1' does not contribute to viral replication *in vitro*, JEV NS1' mutants
130 have less infectivity in a cell model (47, 48). Therefore, the role of NS1' in the JEV life
131 cycle and pathogenesis remains unclear.

132 Here, we report the crystal structure of the C-terminal domain (amino acids 172-
133 352) of JEV NS1 and compare it with published DENV, WNV, and ZIKV NS1 structures.
134 Our findings reveal a diversity in protein surface charges. Furthermore, the solution
135 conformation of the protein was examined by small-angle X-ray scattering (SAXS) and
136 molecular dynamics (MD) simulations along with analysis of cell membrane association.
137 Importantly, we define a cross-reactive epitope on NS1 using an antibody that shows
138 protective activity against WNV infection. Our study shows the common and contrasting

139 features of flavivirus NS1 structure, which contributes to our knowledge of the molecular
140 basis of multiple NS1 functions.
141

142 **Results**

143 **Structure of C-terminal domain of JEV NS1 and NS1'.** The crystal structure of
144 the C-terminal region of JEV NS1 determined at 2.1 Å resolution is similar by fold to all
145 previously solved flavivirus NS1 structures (**Fig. 2a**). The electron density is visible for
146 residues 177-352, whereas the first 5 residues at the N-terminus are not visible. The
147 monomer consists of 10 β-strands on one side and 4 helices and unstructured loops on
148 the other side. Between each β-strand are β-turns and short loops, apart from β4 and
149 β5 which are separated by a long unstructured loop (residues 218-273) (**Fig. 2a-b**). The
150 protein contains four conserved disulfide bonds (C179-C229, C280-C329, C291-C312,
151 and C313-C316) and hydrogen bonds between β-strands and loops. JEV NS1-C forms
152 20 β-strands oriented in a head-to-head arrangement in the dimer, as do ZIKV, WNV,
153 and DENV NS1 with the dimer length of 9.65 nm at its widest point (**Fig. 2c**). The dimer
154 interface is created by 21 residues from each monomer with an average distance of 2.9
155 Å (**Tables 1 and 2**). Eight of these interface residues are conserved among flavivirus
156 NS1 (**Table 1**, score 7-9). The dimer is connected by 12 hydrogen bonds. When
157 comparing the hydrogen bonding network at the dimer interface of the C-terminal
158 domains of ZIKV (PDB ID 5IY3), WNV (4OIE), and DENV NS1 (4OIG), there are 6
159 common residues with the same bond arrangement: Thr (JEV, ZIKV, WNV)/Ala (DENV)
160 186 , Val (JEV, ZIKV, WNV)/Ile (DENV) 188, Thr (JEV, WNV)/Ser (ZIKV, DENV) 228,
161 His 254, and Thr 230 –Trp 232 (**Tables 1, 2, 3, and Fig. 3**). In addition, we solved the
162 structure of JEV NS1'-C, which is distinguished from NS1 by an extra 52 amino acids
163 from the C terminus of the protein, to 2.6 Å resolution. The structure revealed the same
164 protein fold and dimer orientation. However, it showed only 2 extra amino acids in

165 comparison with the C-terminal domain of JEV NS1 (0.348 Å C α RMSD) (data not
166 shown). The C-terminus is disordered, so the electron density is not visible.

167 **Solution model of JEV NS1-C dimer.** The dimeric nature of JEV NS1-C was
168 confirmed by SAXS studies performed on the protein in solution. The SAXS profiles
169 calculated from the monomer and dimer of JEV NS1-C crystal structure were compared
170 with the JEV NS1-C experimental SAXS data (**Fig. 4a**). A monomer of JEV NS1-C
171 yielded a poor fit to the experimental data with χ of 14.11, whereas a dimer provided an
172 improved fit with χ of 4.02. The radius of gyration of 27.02 Å was obtained from Guinier
173 analysis, which agrees with the value extracted from the pair distribution function, 27.08
174 Å. The pair distribution function of JEV NS1-C shows characteristics of a lengthy ovoid
175 particle with the maximum intra-particle distance (D_{\max}) of 94.1 Å, similar to the widest
176 point of JEV NS1-C dimer crystal structure (96.5 Å) (**Fig. 2c and 4b**). The calculated
177 molecular mass was 45.5 kDa, corresponding to the dimeric form of C-terminus NS1.
178 An averaged *ab initio* model was generated at 30 Å resolution with good similarity
179 agreement (normal spatial discrepancy (NSD) = 0.513 ± 0.016) and compared with the
180 JEV NS1-C dimer crystal structure (**Fig 4c**). The structures are well-matched although
181 there is an extra region of mass near the dimer interface in the SAXS model (labelled M,
182 **Fig. 4c**). This feature also is seen in the SAXS model of WNV, suggesting the NS1
183 crystal structures of JEV and WNV may not fully represent the structure of the protein in
184 solution (21). Analysis of the crystallographic atomic mean-square displacements or B-
185 factors in our JEV NS1-C crystal structure indicates that surface regions of loop 218-
186 272, particularly sub-loop 235-237, have high conformational freedom within the crystal
187 lattice (**Fig. 4d-e**). A 40 nanosecond all atom molecular dynamics (MD) simulation of the

188 JEV NS1-C dimer at 37°C confirmed that movement of this loop is unrestrained in both
189 monomers (**Fig. 4d-e**). We hypothesized that the apparent extra region of mass
190 observed in the JEV NS1-C and WNV SAXS structures could be accounted for by the
191 dynamic nature of the loop 218-272 and the resulting expansion of volume in the
192 solution structures. To model JEV NS1-C behaviour in solution more accurately we
193 created a pool of possible structures with varying loop 218-272 conformations and
194 compared them with our SAXS data. Using this approach, we improved the fit to the
195 experimental SAXS data from χ of 4.02 to 1.48 (**Fig 4a**).

196 **Comparison of JEV NS1-C with other flavivirus NS1-C structures.** JEV NS1-
197 C has the same fold as ZIKV (2.2 Å resolution), WNV (2.6 Å resolution), DENV (3 Å
198 resolution), and superposition gives C α RMSD closest to WNV NS1 (1.162 Å for ZIKV,
199 0.959 Å for WNV, and 1.333 Å for DENV) (**Fig. 2c**). The structural superimposition
200 showed low positional conservation only at the N-terminus, C-terminus, and β -turns.
201 The electrostatic surface potential maps of known NS1-C domains (ZIKV, WNV, and
202 DENV) showed symmetric patterns consistent with homodimers. On the β -ladder
203 surface, all displayed neutral charge in the central regions flanked by negatively
204 charged regions (**Fig. 5**). This negatively charged region is small in DENV, larger in
205 WNV, and expanded diagonally from the top left to bottom right in JEV and ZIKV.
206 Adjacent to it, toward the ends, are small positively charged pockets that are seen
207 clearly only in JEV and ZIKV, and the tips of all NS1-C have mixed charge. The loop
208 surface is more variable than the ladder surface. DENV has a distinct positively charged
209 central region, whereas JEV and WNV have negative charge in their central area. ZIKV
210 is different, as the middle region displays both positive and negative charge. The

211 adjacent area has positively charged pockets in all NS1 structures (**Fig. 5, Table 4**).
212 Three pockets are found in WNV and DENV, whereas ZIKV has only pockets 1 and 2,
213 and JEV has pockets 1 and 3. The residues building the positively charged pockets are
214 conserved in pocket 1 and partially conserved in pocket 2, pocket 3, and front pocket on
215 ladder surface (**Fig. 5b, Table 4**).

216 **Cell membrane interaction via GAGs determination.** Sulfate molecules were
217 found on the surface of JEV NS1-C (**Fig. 6, Table 5**) similar to ZIKV (PDB ID 5K6K),
218 WNV (4O6C), and DENV (4OIG). Moreover, they are distributed near the positively
219 charged pockets. Hence, it is possible that this positively charged area is the binding
220 site of negatively charged ligands. Sulfate containing molecules, such as GAGs, which
221 are involved in NS1-dependent membrane attachment (32), could interact here. To test
222 if the interaction with GAGs occurs via sulfate binding sites at the C-terminus, JEV NS1-
223 C binding to heparin agarose beads was analysed. However, the 20 kDa JEV NS1-C
224 was found only in the flow-through and wash fractions (**Fig. 7a**) indicating that it did not
225 interact efficiently with heparin. The interaction of heparan sulfate, chondroitin sulfate,
226 and dermatan sulfate polymers with JEV NS1-C was investigated by protein thermal
227 shift assay. No JEV NS1-C stabilizing effect was observed for any of GAG polymers
228 tested even at high concentration of GAG (100 μ M). The absence of GAG binding was
229 consistent with the pull-down experiments.

230 An interaction of JEV NS1-C with lipids common to cell membranes was tested
231 using a liposome binding assay. JEV NS1-C did not associate with liposomes at either
232 pH 7.5 and 5.5 (**Fig. 7b**). As full-length NS1 can bind liposomes (22, 49), it appears that
233 the NS1 C-terminus is not responsible for membrane binding. We note that the

234 hydrophobic residues of β -roll and wing domains have been suggested to play a role in
235 membrane binding (22-24).

236 **JEV NS1-C and JEV NS1'-C complexed with 22NS1 Fab.** Comparison of the
237 22NS1 antibody epitope of WNV-NS1-C with JEV NS1-C showed that 9 of 16 residues
238 (Trp232, Ser239, Tyr260, Lys261, Thr262, Glu289, Arg294, Arg314, and Ser315) are
239 conserved between the two viruses (**Fig. 1**) (36). Indeed, 22NS1 mAb cross-reacts with
240 JEV NS1-C and NS1'-C protein, which was confirmed by Western Blotting analysis (**Fig.**
241 **8, lower left inset**) and size exclusion chromatography (**Fig. 8**). JEV NS1-C and 22NS1
242 Fab alone eluted at retention time of 7.9 and 8.3 min, respectively. JEV NS1-C
243 incubated with 22NS1 Fab eluted faster at a retention time of 6.9 min corresponding to
244 complex formation with a small amount of free 22NS1 Fab fragments left. The eluted
245 fraction was analyzed by SDS-PAGE and 2 peaks representing JEV NS1-C and 22NS1
246 (~25 kDa) were identified. This confirms that NS1 and 22NS1 mAb interact in solution
247 (**Fig. 8, lower right inset**). The incubation also generates a small peak at retention time
248 of 6.1 min. This may represent a higher order oligomer of JEV NS1-C, which recruits
249 multiple 22NS1 monomers into a complex which higher hydrodynamic radius than the
250 2:2 complex observed at 6.9 min. In support of this idea, we note the absence of the
251 NS1-C species eluting at ~7.4 min in the complex chromatogram. The protein-Fab
252 complex also was analysed by SAXS. The complex experimental profile was compared
253 to the WNV NS1-C-22NS1 complex (PDB ID 4OII) calculated SAXS scattering profile
254 (**Fig. 9a and c**). The complex (4OII) however, gave a poor fit to the experimental SAXS
255 data with χ of 6.82. Guinier analysis gave the radius of gyration of $52.89 \pm 0.34 \text{ \AA}$, which
256 coincides with 52.50 \AA extracted from the pair distribution function. The pair distribution

257 function of the complex has multiple peaks which signify the multi-domain geometric
258 shape with D_{\max} of 154.9 Å (**Fig. 9b**). The calculated molecular mass was 149.96 kDa.
259 An averaged *ab initio* model was generated at 30 Å resolution. The Fab part of WNV
260 complex (4OII) did not fit into the SAXS envelope and shifted from the positions in 4OII
261 model, whereas the WNV NS1-C dimer fit well (**Fig. 9c-e**) indicating flexibility of Fab
262 epitope in solution. We generated a pseudo-atomic model of the JEV NS1-C antibody
263 complex by replacing the WNV-NS1-C with JEV NS1-C and optimizing the position of
264 the Fab molecules. This model with the 2 Fab molecules shifted away from its primary
265 location in 4OII model had better fit to the SAXS data (χ of 6.82 to 3.09; **Fig. 9a, 9c-e**).
266 Both JEV NS1-C and NS1'-C are able to cross-interact with the protective WNV 22NS1
267 mAb in which JEV NS1-C interact with some flexibility.

268 **Discussion**

269 Flavivirus NS1 proteins have generated much interest because of their multiple
270 functions in viral replication, cell signaling, and immune evasion. Since 2014, the
271 structures of nine NS1 proteins have been solved (21-24, 50). These proteins were
272 expressed in bacterial or insect cell expression systems. Here, we expressed JEV NS1
273 C-terminus in *E. coli* after the failure of several attempts to express full-length JEV NS1
274 in *E. coli*, insect cells, and mammalian cells. We describe the first structure of *E. coli*
275 expressed JEV NS1 C-terminus, which when compared to other NS1 structures as well
276 as JEV NS1'-C, shows a high degree of structural conservation. As expected for NS1',
277 the same fold could explain the similar functions *in vitro* of NS1 and NS1'. However, the
278 specific role of the extra amino acids is not clear yet, although WNV lacking the NS1'
279 form are less neuroinvasive (43).

280 The availability of WNV, DENV, and ZIKV NS1 structures has allowed us to
281 assess similarity and differences which may be relevant to their functional behavior. All
282 NS1 proteins are dimeric *in crystallo*, even though the recombinant protein contains only
283 the C-terminal domain (21, 23). The molecular mass and low resolution model
284 generated from SAXS data confirm the dimeric nature of the isolated C-terminal domain
285 in solution. In contrast to previous work, which suggested that the β -roll domain is
286 responsible for dimerization (49), we propose that 6 common residues which form
287 hydrogen bonds at the dimer interface of all NS1 structures mediate dimer formation
288 (49). In principle, inhibition of dimer formation by interposing a ligand at this site could
289 facilitate anti-flavivirus drug development.

290 Both faces of the JEV NS1-C dimer display electrostatic surface charge diversity.
291 However, when considering the full-length flavivirus NS1 protein structure (22-24), the
292 ladder face of the C-terminal domain is positioned underneath the β -roll domain. The N-
293 terminus protects the central region of the ladder face from the environment. Besides
294 that, the β -roll domain is contained by a hydrophobic region that is suspected to interact
295 with the cell membrane or form a lipid cargo pore in NS1 hexamer making it harder for
296 the ladder face to make an interaction. This model conflicts with a suggestion that the β -
297 ladder might bind to the complement control protein domain (sushi domain) of
298 complement proteins (51). In comparison, the loop face in the JEV NS1-C is fully
299 exposed with its diverse surface charge when compared to ZIKV, WNV, and DENV.
300 Particularly, DENV has the most distinct positive central area whereas the rest are
301 negatively charged. Positively charged pockets found on the loop face of the NS1
302 crystal structure could mediate anionic ligand binding. Moreover, the pockets, especially
303 pocket 1, are composed of conserved sequences and are found in all known NS1
304 structures. The presence or absence of each pocket in NS1 from different flaviviruses
305 may confer upon the individual NS1 proteins the ability to interact with different target
306 proteins or ligands in a virus-specific manner. Sulfate molecules distributed on the NS1
307 surface agree with previous findings for DENV and ZIKV and indicate the potential for
308 anionic ligand interaction. We thought that NS1 might interact with uninfected cell
309 membranes via these sulfate binding sites (32), but further experiments confirmed that
310 JEV NS1-C cannot bind efficiently to heparin, heparan sulfate, chondroitin sulfate, or
311 dermatan sulfate polymers. Thus, the sulfate binding sites are not GAG binding
312 interfaces and could represent a crystallographic artifact. Moreover, JEV NS1-C cannot

313 bind to liposomes. Our results also suggest that NS1 C-terminal is not responsible for
314 binding to the cell membrane through GAGs. Instead, cell membrane interactions may
315 occur at the β -roll and wing domains, as was suggested previously (22-24).

316 B-factor and MD analyses suggest that loop 218-272 is conformationally
317 dynamic. Although the B-factors are high for this region, the X-ray structure does not
318 show disorder. Loop 218-272 links strands β 4 and β 5 and is the longest JEV NS1-C
319 loop. Interestingly, the 22NS1 epitope forms part of this loop (Trp232, Gly235, Ile236,
320 Leu237, Ser239, Asp240, Asn253, Try260, Lys261, and Thr262). Binding with antibody
321 may stabilize the loop as seen in the WNV NS1-C-22NS1 complex (4OII). We suspect
322 that the dynamic 218-272 loop may harbor distinct protein-protein interaction functions,
323 a phenomenon which was found independently in WNV (21). NS1 from other
324 flaviviruses may share this characteristic. Taken together, the models agree that the
325 membrane-associated NS1 dimer orients with the N-terminus facing the endoplasmic
326 reticulum or cell membrane and the loop facing outward (21, 22, 24) making an
327 interacting interface, and likely mediating the biological functions of the protein.
328 Therefore, the loop domain could be a candidate for structure based drug targeting.

329 The anti-WNV NS1 mAb, 22NS1, is protective in mice and did not cross-react
330 with DENV-2 (36). We demonstrated that this mAb can cross-react with the more
331 closely related JEV NS1-C at the same epitope, but with some conformational flexibility.
332 This finding agrees with our MD result showing elasticity in the epitope loop, which may
333 affect the antibody-NS1 structure in solution. Even though the JEV NS1'-C has extra
334 amino acids at the C-terminus, JEV NS1'-C can interact with WNV 22NS1 mAb
335 indicating the C-terminal tail does not obstruct the binding surface of 22NS1. The C-tail

336 may then locate at the side flanking the dimer. The presence of NS1' is a shared
337 characteristic of JE serocomplex viruses, and NS1' may have specific properties that
338 contributes to the propensity of JE serogroup viruses to cause encephalitis.

339 Despite Flavivirus NS1 proteins having a conserved protein fold, these proteins
340 differ in their charge distribution, which may enable unique interactions with host
341 proteins (8, 41). The fact that WNV 22NS1 mAb interacts with JEV NS1 is consistent
342 with close similarity of charge distribution of WNV and JEV NS1. This similarity also
343 extends to ZIKV. Overall, these results provide structural details that aid NS1 function
344 determination and highlight both similarities and contrasts among NS1 orthologs, which
345 may be a productive avenue for developing common diagnostic and therapeutic
346 strategies against this important group of Flavivirus diseases.

347 **Materials and methods**

348 **Protein expression and refolding.** JEV strain SA14 (GenBank: M55506) was
349 used as a template. Synthetic DNA optimized for expression in *E. coli* of JEV NS1 was
350 acquired from Life Technologies. To create JEV NS1-C (amino acid residues 172-352)
351 the target sequences were cloned into pET303 at XbaI/XhoI cloning site by using
352 forward primer 5' gctctagaatgCGTGAAGAAAGCACCGATGAATGTGAT 3', reverse
353 primer 5' ccg ctcgagTTATGCATCAACCTGGCTACGAACCAG 3'. Synthetic *JEVNS1'*
354 was purchased from GenScript (Piscataway, NJ, USA). The full-length NS1' was the
355 NS1 sequence with 156 additional nucleotides. The frameshift sequence was manually
356 added by insertion of thymine at position 3561 as a result of -1 ribosomal frameshifting.
357 JEV NS1'-C were generated from the synthetic *JEVNS1'* by using forward primer 5'
358 gctctagaatgCGTGAAGAAAGCACCGATGAATGTGAT 3', reverse primer 5'
359 ccgctcgagTTAATGCAGATGATAACCCCATGCATctg 3'. Proteins were expressed in *E.*
360 *coli* by autoinduction and refolded by using method modified from previously described
361 in Edeling et al, 2014. The theoretical molecular weight of JEV NS1-C and JEV NS1'-C
362 are 20.54 kDa and 25.98 kDa. Protein yield and purity were analysed by SDS-PAGE.

363 **Protein crystallization and data collection.** JEV NS1-C (~6 mg/ml) and JEV
364 NS1'-C (5-7 mg/ml) were screened using commercial crystallization screens. Successful
365 conditions were optimised by hanging drop method. Needle crystals of C-*JEVNS1* were
366 produced from 1 M Ammonium sulphate and 0.1 M MES pH 5.5. The crystals were flash
367 frozen in reservoir buffer added with 20-25% ethylene glycol. The JEV NS1' -C also
368 crystallized in needle form in 1 M Ammonium sulphate and 5% propanol. The JEV NS1'-
369 C was cryo-protected in reservoir buffer with 20% glycerol.

370 X-ray data were collected at cryogenic temperature, wavelength of 0.98 nm, at
371 beamline PROXIMA 1 at Soleil synchrotron, France and at beamline I02 at Diamond
372 Light Source, UK. Data reduction was carried out by XDS programs (52) or iMosflm
373 (53). The protein structure was determined by molecular replacement using the
374 structure of WNV NS1 C-terminal domain (PDB: 4OIE, sequence identity >70%) as a
375 starting model by MOLREP (54) in the CCP4 program suit. The structure was refined by
376 REFMAC5 (55) and built in COOT (56). Data collection and refinement statistics are
377 shown in **Table 6** The JEV NS1-C refinement statistic of Ramachandran plot is 95.98%
378 favoured and 0% outliers. MolProbity score is 1.6. The JEV NS1'-C refinement statistic
379 of Ramachandran plot is 94.89% favoured and 0% outliers. MolProbity score is 1.84.

380 **Protein structure analysis.** Assembly analysis was performed by program PISA
381 (57). Conservation scores of residues on protein structures was given by ConSurf (58)
382 using 21 homologous sequences. The input homologous sequences of NS1 C-terminus
383 were searched by the program and existing NS1 structure sequences were added
384 manually. Electrostatic surface maps were generated by using PDB2PQR (59) to
385 convert PDB files into PQR files and Adaptive Poisson-Boltzmann Solver (APBS) for
386 electrostatics calculations (60) without pKa prediction.

387 **JEV NS1 C-terminus-22NS1 complex formation.** Complex formation was
388 confirmed by Western blot analysis, with 22NS1 (36) and goat anti-mouse IgG-HRP
389 (Santa Cruz Biotechnology, sc-2055) used as primary and secondary antibodies,
390 respectively. Purified JEV NS1 C-terminus and 22NS1 fragment antigen-binding (FAb)
391 (prepared from 22NS1 IgG mAb using Pierce™ Fab Preparation Kit, Cat No. 44985)
392 were mixed overnight at 4°C at 1:1 ratio JEV NS1-C to 22NS1 and purified by Agilent

393 Bio SEC-3 4.6 300 or GE Superdex 200 10 300 GL. Eluted fractions were analysed by
394 SDS-PAGE.

395 **SAXS data collection and processing.** The JEV NS1-C at a concentration of
396 3.4 mg/ml and JEV NS1-C-22NS1 Fab complex at concentration of 3 mg/ml in TBS
397 buffer (20 mM Tris-HCl pH 7.4, 150 mM NaCl) were analyzed with SEC-SAXS on
398 beamline SWING at Soleil synchrotron, France. Samples were loaded onto an Agilent
399 BioSEC-3 4.6/300 column at a flow rate of 0.25 ml/min, 15°C. Data were collected at a
400 distance of 1.8 m and X-ray wavelength of 1 Å. Data processing was conducted in
401 PRIMUS (61). Comparison of scattering profile was done in FoXS (62). *Ab initio* model
402 was the average from 10 (JEV NS1-C) or 20 (protein complex) independent model
403 calculations with (protein complex) or without symmetry (JEV NS1-C) using DAMMIF
404 (63). The model was averaged with DAMAVER (64) and refined with DAMMIN (65). The
405 low resolution model surface representation was created in CHIMERA (66) using
406 'molmap' command. The molecular mass was calculated from Porod volume (67).
407 Molecular dynamics (MD) simulations were performed using GROMACS 4.6.5 and
408 GROMOS96 54A7 force field in a cubic box solvated with single point charge-E water
409 molecules on JEV NS1-C dimers. A neutral charge was introduced at 150 mM NaCl.
410 The distance between JEV NS1-C dimers and the box edge was set to 10 Å. Long
411 range interactions were defined using the particle mesh Ewald algorithm and other non-
412 bonded interactions were restricted to 10 Å. An energy minimization was performed
413 using the steepest descent algorithm followed by a 100 ps NVT ensemble at 310 K and
414 a 200 ps NPT ensemble at 310 K and 1 bar. Production MD was performed at 310 K
415 and 1 bar for 40 ns. C α displacement was calculated with the GROMACS RMSF

416 function. Torsion angle MD was performed with CNS at 100,000 K for 37.5 ps with
417 sampling every 7.5 fs in eight separate simulations. The best structure was found with
418 FoXS using experimental data over data range $0.017 < q < 0.25 \text{ \AA}^{-1}$ and was refined with
419 another eight separate 7.5 ps simulations and energy minimization in GROMACS using
420 the procedure described above. Models again were compared with FoXS. Freeing loop
421 214-243 gave a fit with experimental data of 1.66. Expanding the flexible region to 218-
422 272 allowed us to improve the fit to 1.48.

423 **Liposome binding assay.** Liposome preparation was modified from previous
424 publications (49, 68). Liposomes were prepared from cholesterol (CHOL) (Sigma,
425 C8667) and 1,2-Dipalmitoyl-sn-glycero-3-phosphocholine (PC) (Sigma, P4329) at 1:9
426 CHOL to PC (22, 49, 68). CHOL and PC powder were dissolved in chloroform. To
427 achieve total 400 nmol, 40 nmol of CHOL and 360 nmol of PC were mixed together in a
428 2 ml tube, and the lipid mixture was dried under nitrogen gas stream. To hydrate the
429 lipid sheets, 50 μl of buffer (50 mM Bis-Tris pH 5.5, 50 mM $(\text{NH}_4)_2\text{SO}_4$, 10 % glycerol or
430 150 mM KCl, 25 mM Tris-HCl pH 7.5, 1 mM DTT, 0.5 mM EDTA.) was added and
431 incubated at room temperature on a shaker for 30 min. Then, the lipid was sonicated
432 with an exponential probe at amplitude 4 for 30 sec with 30 sec interval on a warmed
433 water bath for 5 times. Liposome binding reaction (50 μl) was setup at 400 nmol, 125
434 nmol and 25 nmol of total lipid and mixed with 5 μg of protein. The reactions were
435 incubated at 37°C for 45 min. After that, the reactions were centrifuged at 16000 x g for
436 30 min at 22°C and the supernatant was transferred to a new tube. The lipid pellet was
437 resuspended in 200 μl buffer and also transferred to a new tube. Liposomes were
438 pelleted again and the supernatant was discarded. The liposome pellet was

439 resuspended in 30 μ l of 1x SDS-PAGE sample buffer. Bovine cytochrome bc1 complex,
440 membrane proteins, was used as positive control in 25 mM phosphate buffer pH 7.5,
441 100 mM NaCl, 3 mM NaN₃, 0.015 % DDM buffer. The supernatant and pellet fractions
442 were analyzed by SDS-PAGE.

443 **Heparin binding assay.** Small scale 50 μ l column was setup in pipette tip by
444 using heparin agarose beads (Affi-Gel heparin gel, BIO-RAD). The binding buffer was
445 20 mM HEPES pH 7.4, 150 mM NaCl, and the elution buffer was 20 mM HEPES pH 7.4
446 supplemented with 1.5 M and 2 M NaCl. The column was equilibrated with 400 μ l of
447 binding buffer. JEV NS1-C (5 μ g) was applied to the column and incubated on a roller
448 for 30 min at 4°C. The column was washed with 400 μ l binding buffer 3 times before
449 eluted twice with 100 μ l of 1.5 M and 2 M NaCl elution buffer. Superoxide Dismutase 3
450 (SOD3), which contain heparin binding domain, was used as positive control. Samples
451 from each step: load, flow-through, wash, and elute, were analysed by SDS-PAGE.

452 **Differential scanning fluorimetry (DSF).** Polymers of heparan sulfate (average
453 molecular weight 30,000), chondroitin sulfate (62% chondroitin 4-sulfate and 33%
454 chondroitin 6-sulfate, average molecular weight 45,400), and dermatan sulfate (average
455 molecular weight 41,000) from Iduron at final concentration of 100, 50, 25, 10, 5, 1, 0.5
456 μ M were mixed with JEV NS1-C and Sypro Orange 5000X (Invitrogen) at final
457 concentration of 10 μ M and 10X, respectively. The reaction volume was 10 μ l The
458 experiments were set in 96 well-plates and performed using StepOnePlus™ Real-Time
459 PCR Systems (software version 2.3) (Applied Biosystems). The reactions were
460 equilibrated at 25 °C for 2 min followed by increase to 95 °C at 1 °C min⁻¹. The
461 experiments were performed in three replicates.

462

463 **Acknowledgements**

464 This work was supported by Mahidol-Liverpool Stang Mongkolsuk PhD
465 scholarship. We acknowledge the help from colleagues at the University of Liverpool:
466 Richard Strange, for assistance with electrostatic surface map; Sujitra Keadsanti for
467 assistance with Western Blotting analysis; Kangsa Ampornnanai for providing bovine
468 cytochrome *bc1*; Varunya Chantadol for providing human SOD3; and Pawin Ngamlert
469 for assistance with heparin binding assay. We also thank Samar Hasnain for support
470 and interest in the project throughout and for extensive discussions of the results. We
471 acknowledge the Synchrotron Soleil for the provision of Proxima 1 beamline and SAXS
472 facilities. Use of SOLEIL was funded by the European Community's Seventh
473 Framework Programme (FP7/2007-2013) under BioStruct-X (grant agreement number
474 283570 and proposal number 6714) and HHSN272201400018C (to M.S.D). We
475 gratefully acknowledge the Diamond Synchrotron for the providing support at the I02
476 beamline.

477

478 **Author contributions**

479 T.S. and S.V.A. originated and designed the project; T.P. expressed and purified
480 proteins; T.P. and G.S.A.W performed the experiments; T.P., G.S.A.W., and S.V.A.
481 undertook data analysis; T.P., G.S.A.W., M.S.D., T.S., L.T., and S.V.A. contributed to
482 interpretation of data and wrote the manuscript.

483 Data deposition: The atomic coordinates and structure factors have been deposited in
484 the Protein Data Bank, www.pdb.org (PDB ID **5O19** for JEV NS1-C and **5O36** for JEV
485 NS1'-C)
486

487 **References**

- 488
- 489 1. **Lindenbach BD, Rice CM.** 1997. trans-Complementation of yellow fever virus NS1 reveals a role
- 490 in early RNA replication. *J Virol* **71**:9608-9617.
- 491 2. **Mackenzie JM, Jones MK, Young PR.** 1996. Immunolocalization of the dengue virus
- 492 nonstructural glycoprotein NS1 suggests a role in viral RNA replication. *Virology* **220**:232-240.
- 493 3. **Muylaert IR, Chambers TJ, Galler R, Rice CM.** 1996. Mutagenesis of the N-linked glycosylation
- 494 sites of the yellow fever virus NS1 protein: effects on virus replication and mouse
- 495 neurovirulence. *Virology* **222**:159-168.
- 496 4. **Youn S, Ambrose RL, Mackenzie JM, Diamond MS.** 2013. Non-structural protein-1 is required
- 497 for West Nile virus replication complex formation and viral RNA synthesis. *Virology* **456**:339.
- 498 5. **Fan J, Liu Y, Yuan Z.** 2014. Critical role of Dengue Virus NS1 protein in viral replication. *Virology* **477**:162-169.
- 500 6. **Lindenbach BD, Rice CM.** 1999. Genetic interaction of flavivirus nonstructural proteins NS1 and
- 501 NS4A as a determinant of replicase function. *J Virol* **73**:4611-4621.
- 502 7. **Youn S, Li T, McCune BT, Edeling MA, Fremont DH, Cristea IM, Diamond MS.** 2012. Evidence for
- 503 a genetic and physical interaction between nonstructural proteins NS1 and NS4B that modulates
- 504 replication of West Nile virus. *J Virol* **86**:7360-7371.
- 505 8. **Krishna VD, Rangappa M, Satchidanandam V.** 2009. Virus-specific cytolytic antibodies to
- 506 nonstructural protein 1 of Japanese encephalitis virus effect reduction of virus output from
- 507 infected cells. *J Virol* **83**:4766-4777.
- 508 9. **Winkler G, Randolph VB, Cleaves GR, Ryan TE, Stollar V.** 1988. Evidence that the mature form
- 509 of the flavivirus nonstructural protein NS1 is a dimer. *Virology* **162**:187-196.
- 510 10. **Schlesinger JJ, Brandriss MW, Putnak JR, Walsh EE.** 1990. Cell surface expression of yellow
- 511 fever virus non-structural glycoprotein NS1: consequences of interaction with antibody. *J Gen*
- 512 *Virology* **71 (Pt 3)**:593-599.
- 513 11. **Lee JM, Crooks AJ, Stephenson JR.** 1989. The synthesis and maturation of a non-structural
- 514 extracellular antigen from tick-borne encephalitis virus and its relationship to the intracellular
- 515 NS1 protein. *J Gen Virol* **70 (Pt 2)**:335-343.
- 516 12. **Avirutnan P, Hauhart RE, Somnuk P, Blom AM, Diamond MS, Atkinson JP.** 2011. Binding of
- 517 flavivirus nonstructural protein NS1 to C4b binding protein modulates complement activation. *J*
- 518 *Immunol* **187**:424-433.
- 519 13. **Avirutnan P, Fuchs A, Hauhart RE, Somnuk P, Youn S, Diamond MS, Atkinson JP.** 2010.
- 520 Antagonism of the complement component C4 by flavivirus nonstructural protein NS1. *J Exp*
- 521 *Med* **207**:793-806.
- 522 14. **Chung KM, Liszewski MK, Nybakken G, Davis AE, Townsend RR, Fremont DH, Atkinson JP,**
- 523 **Diamond MS.** 2006. West Nile virus nonstructural protein NS1 inhibits complement activation
- 524 by binding the regulatory protein factor H. *Proc Natl Acad Sci U S A* **103**:19111-19116.
- 525 15. **Morrison CR, Scholle F.** 2014. Abrogation of TLR3 inhibition by discrete amino acid changes in
- 526 the C-terminal half of the West Nile virus NS1 protein. *Virology* **456-457**:96-107.
- 527 16. **Glasner DR, Ratnasiri K, Puerta-Guardo H, Espinosa DA, Beatty PR, Harris E.** 2017. Dengue virus
- 528 NS1 cytokine-independent vascular leak is dependent on endothelial glycocalyx components.
- 529 *PLoS Pathog* **13**:e1006673.
- 530 17. **Modhiran N, Watterson D, Blumenthal A, Baxter AG, Young PR, Stacey KJ.** 2017. Dengue virus
- 531 NS1 protein activates immune cells via TLR4 but not TLR2 or TLR6. *Immunol Cell Biol*
- 532 doi:10.1038/icc.2017.5.

- 533 18. **Modhiran N, Watterson D, Muller DA, Panetta AK, Sester DP, Liu L, Hume DA, Stacey KJ, Young**
534 **PR.** 2015. Dengue virus NS1 protein activates cells via Toll-like receptor 4 and disrupts
535 endothelial cell monolayer integrity. *Sci Transl Med* **7**:304ra142.
- 536 19. **Han YW, Choi JY, Uyangaa E, Kim SB, Kim JH, Kim BS, Kim K, Eo SK.** 2014. Distinct dictation of
537 Japanese encephalitis virus-induced neuroinflammation and lethality via triggering TLR3 and
538 TLR4 signal pathways. *PLoS Pathog* **10**:e1004319.
- 539 20. **Muller DA, Young PR.** 2013. The flavivirus NS1 protein: molecular and structural biology,
540 immunology, role in pathogenesis and application as a diagnostic biomarker. *Antiviral Res*
541 **98**:192-208.
- 542 21. **Edeling MA, Diamond MS, Fremont DH.** 2014. Structural basis of Flavivirus NS1 assembly and
543 antibody recognition. *Proc Natl Acad Sci U S A* **111**:4285-4290.
- 544 22. **Akey DL, Brown WC, Dutta S, Konwerski J, Jose J, Jurkiw TJ, DelProposto J, Ogata CM, Skiniotis**
545 **G, Kuhn RJ, Smith JL.** 2014. Flavivirus NS1 structures reveal surfaces for associations with
546 membranes and the immune system. *Science* **343**:881-885.
- 547 23. **Xu X, Song H, Qi J, Liu Y, Wang H, Su C, Shi Y, Gao GF.** 2016. Contribution of intertwined loop to
548 membrane association revealed by Zika virus full-length NS1 structure. *EMBO J*
549 doi:10.15252/embj.201695290.
- 550 24. **Brown WC, Akey DL, Konwerski JR, Tarrasch JT, Skiniotis G, Kuhn RJ, Smith JL.** 2016. Extended
551 surface for membrane association in Zika virus NS1 structure. *Nat Struct Mol Biol* **23**:865-867.
- 552 25. **Blitvich BJ, Scanlon D, Shiell BJ, Mackenzie JS, Pham K, Hall RA.** 2001. Determination of the
553 intramolecular disulfide bond arrangement and biochemical identification of the glycosylation
554 sites of the nonstructural protein NS1 of Murray Valley encephalitis virus. *J Gen Virol* **82**:2251-
555 2256.
- 556 26. **Mandl CW, Heinz FX, Stockl E, Kunz C.** 1989. Genome sequence of tick-borne encephalitis virus
557 (Western subtype) and comparative analysis of nonstructural proteins with other flaviviruses.
558 *Virology* **173**:291-301.
- 559 27. **Watterson D, Modhiran N, Young PR.** 2016. The many faces of the flavivirus NS1 protein offer a
560 multitude of options for inhibitor design. *Antiviral Res* **130**:7-18.
- 561 28. **Gutsche I, Coulibaly F, Voss JE, Salmon J, d'Alayer J, Ermonval M, Larquet E, Charneau P, Krey**
562 **T, Megret F, Guittet E, Rey FA, Flamand M.** 2011. Secreted dengue virus nonstructural protein
563 NS1 is an atypical barrel-shaped high-density lipoprotein. *Proc Natl Acad Sci U S A* **108**:8003-
564 8008.
- 565 29. **Jacobs MG, Robinson PJ, Bletchly C, Mackenzie JM, Young PR.** 2000. Dengue virus
566 nonstructural protein 1 is expressed in a glycosyl-phosphatidylinositol-linked form that is
567 capable of signal transduction. *FASEB J* **14**:1603-1610.
- 568 30. **Noisakran S, Dechtawewat T, Avirutnan P, Kinoshita T, Siripanyaphinyo U, Puttikhunt C,**
569 **Kasinrerker W, Malasit P, Sittisombut N.** 2008. Association of dengue virus NS1 protein with lipid
570 rafts. *J Gen Virol* **89**:2492-2500.
- 571 31. **Noisakran S, Dechtawewat T, Rinkaewkan P, Puttikhunt C, Kanjanahaluethai A, Kasinrerker W,**
572 **Sittisombut N, Malasit P.** 2007. Characterization of dengue virus NS1 stably expressed in 293T
573 cell lines. *J Virol Methods* **142**:67-80.
- 574 32. **Avirutnan P, Zhang L, Punyadee N, Manuyakorn A, Puttikhunt C, Kasinrerker W, Malasit P,**
575 **Atkinson JP, Diamond MS.** 2007. Secreted NS1 of dengue virus attaches to the surface of cells
576 via interactions with heparan sulfate and chondroitin sulfate E. *PLoS Pathog* **3**:e183.
- 577 33. **Li YZ, Counor D, Lu P, Liang GD, Vu TQ, Phan TN, Huynh TK, Sun G, Grandadam M, Butrapet S,**
578 **Lavergne JP, Flamand M, Yu YX, Solomon T, Buchy P, Deubel V.** 2012. A specific and sensitive
579 antigen capture assay for NS1 protein quantitation in Japanese encephalitis virus infection. *J*
580 *Virol Methods* **179**:8-16.

- 581 34. **Amorim JH, Alves RP, Boscardin SB, Ferreira LC.** 2014. The dengue virus non-structural 1
582 protein: risks and benefits. *Virus Res* **181**:53-60.
- 583 35. **Solomon T, Thao LT, Dung NM, Kneen R, Hung NT, Nisalak A, Vaughn DW, Farrar J, Hien TT,**
584 **White NJ, Cardoso MJ.** 1998. Rapid diagnosis of Japanese encephalitis by using an
585 immunoglobulin M dot enzyme immunoassay. *J Clin Microbiol* **36**:2030-2034.
- 586 36. **Chung KM, Nybakken GE, Thompson BS, Engle MJ, Marri A, Fremont DH, Diamond MS.** 2006.
587 Antibodies against West Nile Virus nonstructural protein NS1 prevent lethal infection through Fc
588 gamma receptor-dependent and -independent mechanisms. *J Virol* **80**:1340-1351.
- 589 37. **Schlesinger JJ, Brandriss MW, Cropp CB, Monath TP.** 1986. Protection against yellow fever in
590 monkeys by immunization with yellow fever virus nonstructural protein NS1. *J Virol* **60**:1153-
591 1155.
- 592 38. **Schlesinger JJ, Foltzer M, Chapman S.** 1993. The Fc portion of antibody to yellow fever virus NS1
593 is a determinant of protection against YF encephalitis in mice. *Virology* **192**:132-141.
- 594 39. **Li Y, Counor D, Lu P, Duong V, Yu Y, Deubel V.** 2012. Protective immunity to Japanese
595 encephalitis virus associated with anti-NS1 antibodies in a mouse model. *Virol J* **9**:135.
- 596 40. **Liu J, Liu Y, Nie K, Du S, Qiu J, Pang X, Wang P, Cheng G.** 2016. Flavivirus NS1 protein in infected
597 host sera enhances viral acquisition by mosquitoes. *Nat Microbiol* **1**:16087.
- 598 41. **Cheng HJ, Lin CF, Lei HY, Liu HS, Yeh TM, Luo YH, Lin YS.** 2009. Proteomic analysis of endothelial
599 cell autoantigens recognized by anti-dengue virus nonstructural protein 1 antibodies. *Exp Biol*
600 *Med (Maywood)* **234**:63-73.
- 601 42. **Beatty PR, Puerta-Guardo H, Killingbeck SS, Glasner DR, Hopkins K, Harris E.** 2015. Dengue
602 virus NS1 triggers endothelial permeability and vascular leak that is prevented by NS1
603 vaccination. *Sci Transl Med* **7**:304ra141.
- 604 43. **Melian EB, Hinzman E, Nagasaki T, Firth AE, Wills NM, Nouwens AS, Blitvich BJ, Leung J, Funk**
605 **A, Atkins JF, Hall R, Khromykh AA.** 2010. NS1' of flaviviruses in the Japanese encephalitis virus
606 serogroup is a product of ribosomal frameshifting and plays a role in viral neuroinvasiveness. *J*
607 *Virol* **84**:1641-1647.
- 608 44. **Mason PW.** 1989. Maturation of Japanese encephalitis virus glycoproteins produced by infected
609 mammalian and mosquito cells. *Virology* **169**:354-364.
- 610 45. **Young LB, Melian EB, Khromykh AA.** 2013. NS1' colocalizes with NS1 and can substitute for NS1
611 in West Nile virus replication. *J Virol* **87**:9384-9390.
- 612 46. **Ye Q, Li XF, Zhao H, Li SH, Deng YQ, Cao RY, Song KY, Wang HJ, Hua RH, Yu YX, Zhou X, Qin ED,**
613 **Qin CF.** 2012. A single nucleotide mutation in NS2A of Japanese encephalitis-live vaccine virus
614 (SA14-14-2) ablates NS1' formation and contributes to attenuation. *J Gen Virol* **93**:1959-1964.
- 615 47. **Melian EB, Hall-Mendelin S, Du F, Owens N, Bosco-Lauth AM, Nagasaki T, Rudd S, Brault AC,**
616 **Bowen RA, Hall RA, van den Hurk AF, Khromykh AA.** 2014. Programmed ribosomal frameshift
617 alters expression of west nile virus genes and facilitates virus replication in birds and
618 mosquitoes. *PLoS Pathog* **10**:e1004447.
- 619 48. **Takamatsu Y, Okamoto K, Dinh DT, Yu F, Hayasaka D, Uchida L, Nabeshima T, Buerano CC,**
620 **Morita K.** 2014. NS1' protein expression facilitates production of Japanese encephalitis virus in
621 avian cells and embryonated chicken eggs. *J Gen Virol* **95**:373-383.
- 622 49. **Smith JL, AKEY DL, BROWN WC, Kuhn RJ.** 2015. Vaccine compositions and uses thereof WO
623 2015095735 A2. Google Patents.
- 624 50. **Song H, Qi J, Haywood J, Shi Y, Gao GF.** 2016. Zika virus NS1 structure reveals diversity of
625 electrostatic surfaces among flaviviruses. *Nat Struct Mol Biol* **23**:456-458.
- 626 51. **Akey DL, Brown WC, Jose J, Kuhn RJ, Smith JL.** 2015. Structure-guided insights on the role of
627 NS1 in flavivirus infection. *Bioessays* **37**:489-494.
- 628 52. **Kabsch W.** 2010. Xds. *Acta Crystallogr D Biol Crystallogr* **66**:125-132.

- 629 53. **Battye TG, Kontogiannis L, Johnson O, Powell HR, Leslie AG.** 2011. iMOSFLM: a new graphical
630 interface for diffraction-image processing with MOSFLM. *Acta Crystallogr D Biol Crystallogr*
631 **67**:271-281.
- 632 54. **Vagin A, Teplyakov A.** 2010. Molecular replacement with MOLREP. *Acta Crystallogr D Biol*
633 *Crystallogr* **66**:22-25.
- 634 55. **Murshudov GN, Skubak P, Lebedev AA, Pannu NS, Steiner RA, Nicholls RA, Winn MD, Long F,**
635 **Vagin AA.** 2011. REFMAC5 for the refinement of macromolecular crystal structures. *Acta*
636 *Crystallogr D Biol Crystallogr* **67**:355-367.
- 637 56. **Emsley P, Lohkamp B, Scott WG, Cowtan K.** 2010. Features and development of Coot. *Acta*
638 *Crystallogr D Biol Crystallogr* **66**:486-501.
- 639 57. **Krissinel E, Henrick K.** 2007. Inference of macromolecular assemblies from crystalline state. *J*
640 *Mol Biol* **372**:774-797.
- 641 58. **Landau M, Mayrose I, Rosenberg Y, Glaser F, Martz E, Pupko T, Ben-Tal N.** 2005. ConSurf 2005:
642 the projection of evolutionary conservation scores of residues on protein structures. *Nucleic*
643 *Acids Res* **33**:W299-302.
- 644 59. **Dolinsky TJ, Czodrowski P, Li H, Nielsen JE, Jensen JH, Klebe G, Baker NA.** 2007. PDB2PQR:
645 expanding and upgrading automated preparation of biomolecular structures for molecular
646 simulations. *Nucleic Acids Research* **35**:W522-W525.
- 647 60. **Baker NA, Sept D, Joseph S, Holst MJ, McCammon JA.** 2001. Electrostatics of nanosystems:
648 application to microtubules and the ribosome. *Proc Natl Acad Sci U S A* **98**:10037-10041.
- 649 61. **Konarev PV, Volkov VV, Sokolova AV, Koch MHJ, Svergun DI.** 2003. PRIMUS: a Windows PC-
650 based system for small-angle scattering data analysis. *Journal of Applied Crystallography*
651 **36**:1277-1282.
- 652 62. **Schneidman-Duhovny D, Hammel M, Tainer JA, Sali A.** 2013. Accurate SAXS profile
653 computation and its assessment by contrast variation experiments. *Biophys J* **105**:962-974.
- 654 63. **Franke D, Svergun DI.** 2009. DAMMIF, a program for rapid ab-initio shape determination in
655 small-angle scattering. *J Appl Crystallogr* **42**:342-346.
- 656 64. **Volkov VV, Svergun DI.** 2003. Uniqueness of ab initio shape determination in small-angle
657 scattering. *Journal of Applied Crystallography* **36**:860-864.
- 658 65. **Svergun DI.** 1999. Restoring low resolution structure of biological macromolecules from solution
659 scattering using simulated annealing. *Biophysical Journal* **76**:2879-2886.
- 660 66. **Pettersen EF, Goddard TD, Huang CC, Couch GS, Greenblatt DM, Meng EC, Ferrin TE.** 2004.
661 UCSF Chimera--a visualization system for exploratory research and analysis. *J Comput Chem*
662 **25**:1605-1612.
- 663 67. **Petoukhov MV, Franke D, Shkumatov AV, Tria G, Kikhney AG, Gajda M, Gorba C, Mertens HDT,**
664 **Konarev PV, Svergun DI.** 2012. New developments in the ATSAS program package for small-
665 angle scattering data analysis. *Journal of Applied Crystallography* **45**:342-350.
- 666 68. **Julkowska MM, Rankenberg JM, Testerink C.** 2013. Liposome-binding assays to assess
667 specificity and affinity of phospholipid-protein interactions. *Methods Mol Biol* **1009**:261-271.
- 668
- 669
- 670

671 **FIGURE LEGENDS**

672 **Figure 1. Sequence alignment of full-length Flavivirus NS1 produced from**
673 **Clustal W (1).** An asterisk indicates fully conserved residue. A colon indicates
674 conservation between groups of strongly similar properties. A period indicates
675 conservation between groups of weakly similar properties. The amino acid sequences
676 were used for X-ray structure studies: DENV1 U88535 for PDB ID 4OIG, DENV2
677 M84727 for 4O6B, WNV 196835 for 4O6C and 4OIE, ZIKV KU365779 for 5IY3, and
678 ZIKV AY632535 for 5K6K and 5GS6. The 22NS1 light chain epitopes are highlighted in
679 red and heavy chain epitopes are in black squares.

680 **Figure 2. The C-terminal domain structure of JEV NS1.** (a) Ribbon model of
681 JEV NS1-C monomer. One side is built of 10 β -strands and the opposite is the non-
682 structured loops. Disulfide bonds are shown in yellow. (b) Topology diagram of JEV
683 NS1-C. Four disulfide bonds are indicated as white spheres. β represent the β -sheet
684 and η represent 3₁₀ helix. (c) Superimposed ribbon diagram of NS1-C of JEV
685 (magenta), ZIKV (PDB: 5IY3, blue), WNV (PDB: 4OIE, green), and DENV1 (PDB: 4OIG,
686 gold).

687 **Figure 3. Dimer interface of JEV NS1-C.** (a, b) The surface of 21 residues from
688 one monomer involved in dimer interface is colored in lime green and the surface that
689 form hydrogen bonds are colored in dark green. Similarly, another monomer interfacing
690 surface is in magenta and surface forming hydrogen bonds are in dark magenta. (c)
691 Residues involved in hydrogen formation at the dimer interface are highlighted in lime
692 green and magenta, respectively. Hydrogen bonds are indicated by dashed lines.

693 **Figure 4. Solution model of JEV NS1-C dimer.** (a) SAXS scattering curve.
694 Experimental scattering curve is shown in black scattering. Scattering profile of JEV
695 NS1-C monomer, dimer, and the best molecular dynamic simulation structure calculated
696 with FoXS are shown in blue, green, and red, respectively. (b) Pair distribution functions
697 (c) Low-resolution model of JEV NS1-C calculated from SAXS profiles docked with the
698 crystal structure of the JEV NS1-C dimer. An extra region of mass is labelled with M. (d)
699 RMSF plot of the molecular dynamic simulation at the flexible loop. RMSF values of
700 each monomer are in black and red. Average β -factor of each residue is in grey. (e) The
701 best molecular dynamic simulation structure (red) was superimposed with JEV NS1-C
702 crystal structure (blue). The flexible loop 218-272 shown in yellow.

703 **Figure 5. JEV NS1-C compared to other flavivirus NS1-C structures.** (a)
704 Electrostatic surface map of NS1-C from JEV, ZIKV, WNV, and DENV. Surface is
705 colored by electrostatic potential from -5 kT/e (red) to 5 kT/e (blue). Positive potential
706 pockets are depicted in dash circles. (b) Surface model color-coded by conservation.
707 The most conserved residues are represented in dark magenta and the most variable
708 residues are represented in dark green.

709 **Figure 6. Sulfate molecules bound to the loop surface of JEV NS1-C.** Sulfate
710 molecules were found not only for JEV NS1, but also in DENV 4OIG, ZIKV 5K6K, and
711 WNV 4O6C. Thus, it is suspected to be an importance sulfate binding interface.

712 **Figure 7. Cell membrane interaction via GAG determination.** (a) Heparin
713 binding determination. JEV NS1-C was incubated with heparin agarose beads. Total
714 JEV NS1-C loaded to the column is shown in lane 1. Lane 2 is flow-through fraction.
715 Lane 3-4 are wash fraction. The column was eluted with buffer supplemented with 1.5 M

716 NaCl shown in lane 5. Three independent experiments were conducted. **(b)** Liposome
717 binding assay. The experiments were conducted at pH 7.5 (upper) and pH 5.5 (lower).
718 Supernatant and pellet fractions separated by centrifugation were analysed by SDS-
719 PAGE. Lanes 1, 2, and 3, were pellet of 400 nmol, 100 nmol, and 25 nmol reactions,
720 respectively. Lanes 4, 5, and 6, were supernatant of 400 nmol, 100 nmol, and 25 nmol
721 reactions, respectively. Three independent experiments were conducted.

722 **Figure 8. JEV NS1-C complexed with 22NS1 Fab.** JEV NS1-C was detected by
723 22NS1 mAb (lower left inset). JEV NS1-C was incubated with 22NS1 Fab at 1:1 molar
724 ratio protein to Fab fragment and the complex formation was analysed on an Agilent
725 BioSEC-3 4.6/300. The lower right panel show SDS-PAGE analysis of each elution
726 fraction.

727 **Figure 9. SAXS analysis of JEV NS1-C-22NS1 Fab complex.** **(a)** SAXS
728 scattering curve. Experimental scattering curve of JEV NS1-C-22NS1 Fab complex is
729 shown in black scattering. Calculated scattering profile of WNV NS1-C -22NS1 complex
730 (4OII) is displayed in green, and JEV NS1-C -22NS1 Fab complex manually fit model is
731 shown in orange. **(b)** Pair distribution functions shows multiple peaks signify the multi-
732 domain structure. **(c)** WNV NS1-C-22NS1 complex (4OII). WNV NS1-C is colored in
733 deep sky blue. 22NS1 Fabs are coloured in salmon. **(d)** WNV NS1-C-22NS1 complex
734 (4OII) fit to the JEV NS1-C -22NS1 Fab complex ab initio model (upper). A pseudo-
735 atomic model JEV NS1-C -22NS1 Fab complex are manually fit to the ab initio model
736 (lower). **(e)** JEV NS1-C-22NS1 Fab complex pseudo-atomic model. JEV NS1-C is
737 coloured in light green. 22NS1 Fab is colored in orchid and another Fab is colored in
738 sky blue.

739 **Figure 10. JEV NS1 homology model. JEV NS1 full length model created by**
740 **using SWISS-MODEL** Homology Modelling. Dimerization was generated by
741 superimposition of the JEV NS1 homology model to ZIKV NS1 PDB ID 5GS6. **(a)**
742 Cross-shaped homodimer NS1. One subunit is coloured in grey and another is coloured
743 by domain. β -roll (amino acid residues 1-29) domain is coloured in green, wing (38-151)
744 domain is coloured in blue, and β -ladder domains (181-352) is coloured in brown. **(b)**
745 Side view of NS1. Residues 108-128 of the JEV homology model are indicated in
746 magenta. Residues 108-128 are disordered and not visible in DENV 4O6B, WNV 4O6C,
747 but they are visible in ZIKV 5GS6 (shown in yellow) and 5K6K. Hydrophobic residues
748 (28, 115, 118, 123, and 160-163) suspected to involve with cell membrane interaction
749 are labelled.
750

751 **Table 1 JEV NS1 C-terminus dimer interfacing residues**

Number	Residue	ASA (Å ²) ¹	BSA (Å ²) ²	ΔG (kcal/mol) ³	Conservation ⁴
1	Gly181	23.56	6.81	0.03	3
2	Ala182	91.29	45.68	0.30	1
3	Ile184	22.47	16.36	-0.18	5
4	Gly185	40.33	16.05	0.26	7
5	Thr186	37.46	36.73	-0.22	7
6	Ala187	63.58	21.49	0.34	9
7	Val188	64.98	63.40	0.34	6
8	Lys189	181.59	9.98	0.16	8
9	Gly190	63.17	54.83	0.30	5
10	His191	110.70	33.66	0.74	1
11	Trp210	60.01	29.42	0.08	5
12	Glu227	104.51	54.79	0.51	5
13	Thr228	120.12	94.74	0.66	6
14	His229	54.08	52.04	0.90	9
15	Thr230	24.89	21.26	-0.20	9
16	Leu231	48.09	48.09	0.77	8
17	Trp232	95.68	59.18	0.38	5
18	Gly233	39.95	30.60	-0.02	4
19	Asp234	91.67	54.93	0.26	6
20	Asp235	128.72	0.58	-0.01	1
21	His254	13.56	10.75	0.73	8

752 ¹ ASA= Accessible Surface Area753 ² BSA= Buried Surface Area754 ³ ΔG= Solvation energy effect755 ^{1,2,3} Assembly analysis in the program PISA.756 ⁴ Amino acid conservation score are given by Consurf. (9 = conserved and 1 = variable)

757 **Table 2 Hydrogen bonds between JEV NS1 C-terminus dimer interfacing residues**

758	Number	Structure 1	Distance (Å) ¹	Structure 2
759	1	Gly190 [N]	2.93	Ile184 [O]
760	2	Val188 [N]	2.86	Thr186 [O]
761	3	Thr186 [N]	2.89	Val188 [O]
762	4	His229 [NE2]	2.83	Gly190 [O]
763	5	His254 [NE2]	2.94	Thr228 [O]
764	6	Trp232 [N]	2.96	Thr230 [O]
765	7	Ile184 [O]	2.93	Gly190 [N]
766	8	Thr186 [O]	2.86	Val188 [N]
767	9	Val188 [O]	2.89	Thr186 [N]
768	10	Gly190 [O]	2.83	His229 [NE2]
	11	Thr228 [O]	2.94	His254 [NE2]
	12	Thr230 [O]	2.96	Trp232 [N]

769

770 ¹ Assembly analysis in the program PISA.

771

772 **Table 3 Residues forming hydrogen bond at dimer interface compared with**
 773 **existing flavivirus NS1**

JEV	ZIKV			WNV			DENV	
	5k6k	5gs6	5iy3	4o6d	4o6c	4oie	4o6b	4oig
	Asp1	His1		Asp1	Asp1			
	Val2	Val2		Thr2	Thr2		Ser2	
	Cys4	Cys4		Cys4	Cys4		Cys4	
	Ser5	Ser5						
	Val6	Val6		Ile6	Val6		Ile6	
	Phe8							
	Ser9							
				Arg10	Arg10			
	Lys11							
	Glu12			Glu12	Glu12			
				Leu13				
	Arg14	Arg14		Arg14	Arg14		Lys14	
	Thr17	Thr17		Ser17	Ser17		Ser17	
	Val19	Val19		Val19	Val19		Ile19	
	Phe20	Phe20		Phe20	Phe20			
	Ile21	Val21		Ile21	Ile21		Ile21	
	Tyr22	Tyr22						
	Asn23	Asn23		Asn23	Asn23		Asp23	

JEV	ZIKV			WNV		DENV		
	5k6k	5gs6	5iy3	4o6d	4o6c	4oie	4o6b	4oig
	Asp24	Asp24		Asp24	Asp24			
	Arg31			Arg31	Arg31			
	Tyr32			Tyr32	Tyr32			
	Asp157	Asp157					Tyr158	
				Phe160				
	Thr165			Thr165	Thr165			
				Ser181	Ser181			
				Lys182	Lys182			Arg182
Ile184	Ile184	Ile184	Ile184					
								Ser185
Thr186	Thr186	Thr186	Thr186	Thr186	Thr186	Thr186	Ala186	Ala186
Val188	Val188	Val188	Val188	Val188	Val188	Val188	Ile188	Ile188
	Lys189			Lys189	Lys189			Lys189
Gly190	Gly190	Gly190	Gly190					Asp190
		Lys191		Asn191	Asn191			
	192Glu	Glu192						
	193Ala							
	Glu203			Glu203				
	Lys227	Lys227	Lys227					

JEV	ZIKV			WNV			DENV	
	5k6k	5gs6	5iy3	4o6d	4o6c	4oie	4o6b	4oig
Thr228	Ser228	Ser228	Ser228	Thr228	Thr228	Thr228	Ser228	Ser228
His229	His229	His229	His229					
Thr230	Thr230	Thr230	Thr230	Thr230	Thr230	Thr230	Thr230	Thr230
Trp232	Trp232	Trp232	Trp232	Trp232	Trp232	Trp232	Trp232	Trp232
	Thr233	Thr233	Thr233				Ser233	Ser233
	Asp234	Asp234	Asp234				Asn234	Asn234
His254	His254	His254	His254	His254	His254	His254	His254	His254

774

775 Note: shared residues are shaded in grey.

776 **Table 4 Residues forming positively charge pockets compared to existed C-NS1.**

JEV	ZIKV	WNV	DENV	Conservation¹
	5IY3	4OIE	4OIG	
Pocket 1				
Gly259	Gly259	Gly259	Gly259	9
Tyr260	Tyr260	Tyr260	Tyr260	9
Lys261	Arg261	Lys261	Phe261	1
			Ala265	1
Ser292	Gly292	Gly292	Gly292	1
Lys293	Thr293	His293	Asn293	1
Arg294	Arg294	Arg294	Arg294	9
Cys313				9
Arg314	Arg314	Arg314	Arg314	9
Ser315	Glu315	Ser315	Ser315	5
Cys316	Cys316	Cys316	Cys316	9
Glu334	Glu334	Glu334	Glu334	9
Pocket 2				
	Thr262	Thr262	Thr262	6
	Met264	Asn264	Thr264	1
	Lys265			1
	Gly295	Gly295	Gly295	9
	Pro296	Pro296	Pro296	4
		Gly332		6
	Met333	Met333	Met333	9
	Thr351	Asn351	Ser351	3
Pocket 3				
	Gly295			9
	Pro296			4
	Ser297	Ala297	Ser297	9

JEV	ZIKV	WNV	DENV	Conservation¹
	5IY3	4OIE	4OIG	
Val298		Thr298	Leu298	1
Arg336		Arg336	Arg336	9
Pro337		Pro337	Pro337	9
Met339				3
			Glu340	2
		Glu342	Glu342	8
Leu345		Leu345	Leu345	6
Arg347		Gln347	Lys347	3

777

778 ¹Amino acid conservation score are given by ConSurf. (9 = conserved and 1 = variable)

779 **Table 5 Sulphate contact residues from assembly analysis in the program PISA**

780 (57)

Area	C-JEV	ZIKV	WNV	C-DENV
		5K6K	4O6C	4OIG
Tip	Arg347	Ser342		His309
	Gln349	Glu343		Glu310
	Thr302	Thr302		Lys339
	Ser304	Ser304		
	Lys306	Arg306		
	Thr343			
	Thr344			
Positively charge pockets	Arg294	Arg294		
	Arg314	Arg261		
Central	Asp235		Gly235	His181
				Lys206
				Thr210
				Ser228
				Trp232
				Asn234
				Gly235

781

782

783

784 **Table 6 Data collection and refinement statistics.**

785

	JEV NS1-C	JEV NS1'-C
Data collection		
Space group	I212121	I212121
Cell dimensions		
<i>a, b, c</i> (Å)	49.42, 78.24, 163.18	50.32, 77.94, 163.49
<i>a, b, c</i> (°)	90, 90, 90	90, 90, 90
Resolution (Å)	47.3-2.10 (2.21-2.10)	81.75-2.6 (2.72-2.6)
<i>R</i> _{merge}	0.103 (0.907)	0.2 (1.413)
<i>R</i> _{pim}	0.045 (0.383)	0.141 (1.030)
<i>I</i> / σ <i>I</i>	11.5 (2.3)	7.1 (2.1)
Completeness (%)	99.8 (99.6)	99.9 (99.9)
Redundancy	6.3 (6.5)	5.3 (5.2)
Refinement		
Resolution (Å)	47.3-2.10	81.75-2.6
No. reflections	17944	9719
<i>R</i> _{work} / <i>R</i> _{free}	0.189/0.228	0.166/0.225
No. atoms	1574	1573
Protein	1398	1418
Sulfate ion	60	60
Ligand	24 (MES)	4 (POL)
Water	92	91
<i>B</i> -factors		
Protein	41.516	38.612
Sulfate ion	90.121	85.148
Ligand	86.736 (MES)	61.722 (POL)
Water	50.187	48.669
R.m.s. deviations		
Bond lengths (Å)	0.016	0.016
Bond angles (°)	1.785	1.741

```

170          180          190          200          210
JEV_M55506   K I R E E S T D E C D G A I I G T A V K G H V A V H S D L S Y W I E S R Y N D T W K L E R A V F G E
WNV_AF196835 K V R E S N T T E C D S K I I G T A V K N N L A I H S D L S Y W I E S R L N D T W K L E R A V L G E
ZIKV_KU365779.1 K V R E D Y S L E C D P A V I G T A V K G K E A V H S D L G Y W I E S E K N D T W R L K R A H L I E
ZIKV_AY632535 K V R E D Y S L E C D P A V I G T A V K G R E A A H S D L G Y W I E S E K N D T W R L K R A H L I E
DENT1_U88535  K L R D S Y T Q V C D H R L M S A A I K D S K A V H A D M G Y W I E S E K N E T W K L A R A S F I E
DENV2_M84727  K L K E K Q D V F C D S K L M S A A I K D N R A V H A D M G Y W I E S A L N D T W K I E K A S F I E
DENT3_EF643017 K L R E V Y T Q L C D H R L M S A A V K D E R A V H A D M G Y W I E S Q K N G S W K L E K A S L I E
DENT4_AF326573 K F R E G S S E V C D H R L M S A A I K D Q K A V H A D M G Y W I E S S K N Q T W Q I E K A S L I E
Clustal Consensus * . : : * * : : : * : * . * * : * : * * * * * * * : * : : : * : *

```

```

220          230          240          250          260
JEV_M55506   V K S C T W P E T H T L W G D D V E E S E L I I P H T I A G P K S K H N R R E G Y K T Q N Q G P W D
WNV_AF196835 V K S C T W P E T H T L W G D G I L E S D L I I P V T L A G P R S N H N R R P G Y K T Q N Q G P W D
ZIKV_KU365779.1 M K T C E W P K S H T L W T D G I E E S D L I I P K S L A G P L S H H N T R E G Y R T Q M K G P W H
ZIKV_AY632535 M K T C E W P K S H T L W T D G V E E S D L I I P K S L A G P L S H H N T R E G Y R T Q V K G P W H
DENT1_U88535  V K T C I W P K S H T L W S N G V L E S E M I I P K I Y G G P I S Q H N Y R P G Y F T Q T A G P W H
DENV2_M84727  V K N C H W P K S H T L W S N G V L E S E M I I P K N L A G P V S Q H N Y R P G Y H T Q I T G P W H
DENT3_EF643017 V K T C T W P K S H T L W S N G V L E S D M I T P K S L A G P I S Q H N H R P G Y H T Q T A G P W H
DENT4_AF326573 V K T C L W P K T H T L W S N G V L E S Q M L I P K S Y A G P F S Q H N Y R Q G Y A T Q T V G P W H
Clustal Consensus : * . * * * : : * * * * : : : * : : : * . * * * * : * * * * * * * * * * * * *

```

```

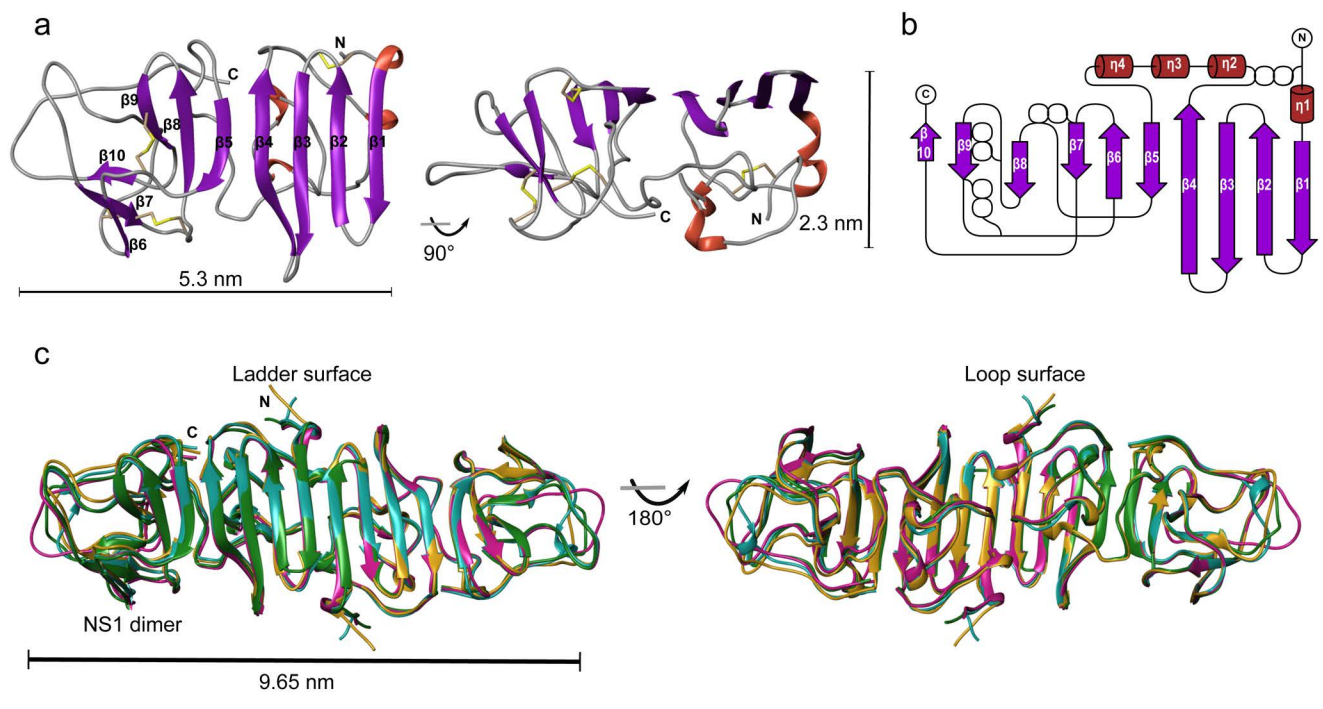
270          280          290          300          310
JEV_M55506   E N G I V L D F D Y C P G T K V T I T E D C S K R I G P S V R T T T D S G K L I T D W C C R S C S L P
WNV_AF196835 E G R V E I D F D Y C P G T T V T L S E S C G H R G P A T R T T T E S G K L I T D W C C R S C T L P
ZIKV_KU365779.1 S E E L E I R F E E C P G T K V H V E E T C G T R G P S L R S T T A S G R V I E E W C C R E C T M P
ZIKV_AY632535 S E E L E I R F E E C P G T K V Y V E E T C G T R G P S L R S T T A S G R V I E E W C C R E C T M P
DENT1_U88535  L G K L E L D F D L C E G T T V V V D E H C G N R G P S L R T T T V T G K T I H E W C C R S C T L P
DENV2_M84727  L G K L E M D F D F C D G T T V V V T E D C G N R G P S L R T T T A S G K L I T E W C C R S C T L P
DENT3_EF643017 L G K L E L D F N Y C E G T T V V I T E N C G T R G P S L R T T T V S G K L I H E W C C R S C T L P
DENT4_AF326573 L G K L E I D F G E C P G T T V T I Q E D C D H R G P S L R T T T A S G K L V T Q W C C R S C T M P
Clustal Consensus : : * * * * * * : * * * * * * * * * * * * * * * * * * * * * * *

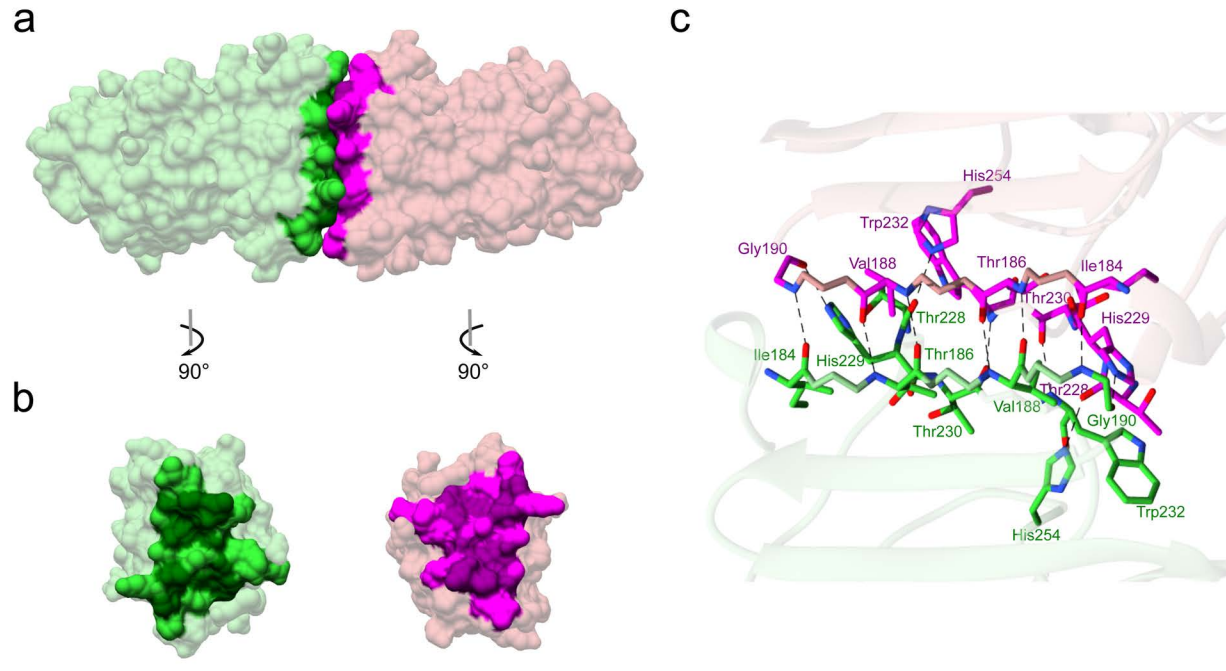
```

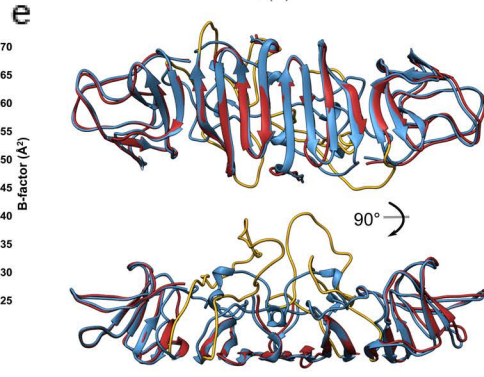
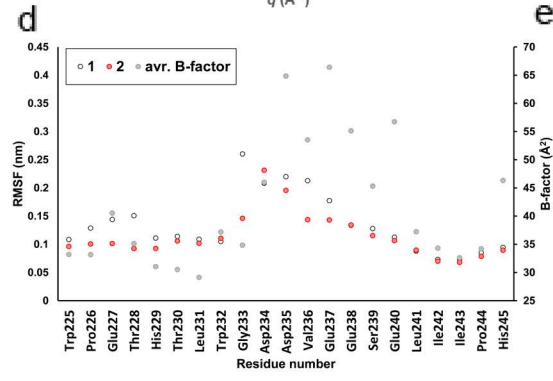
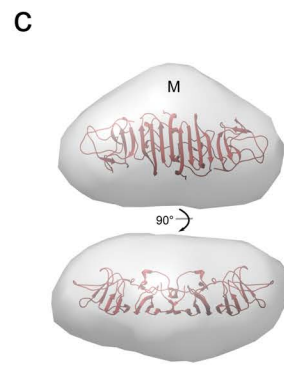
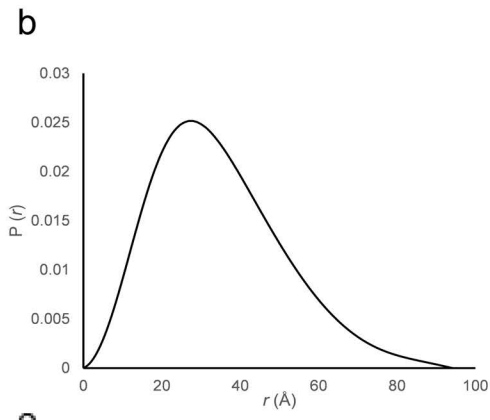
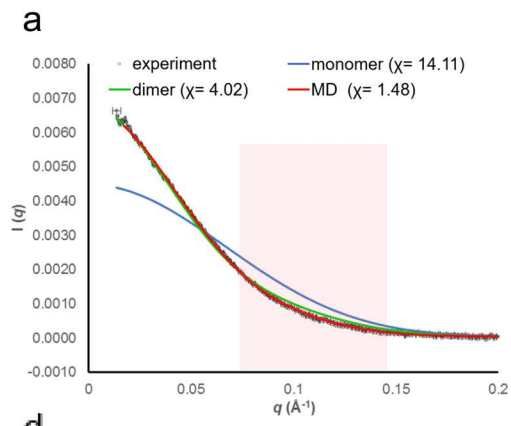
```

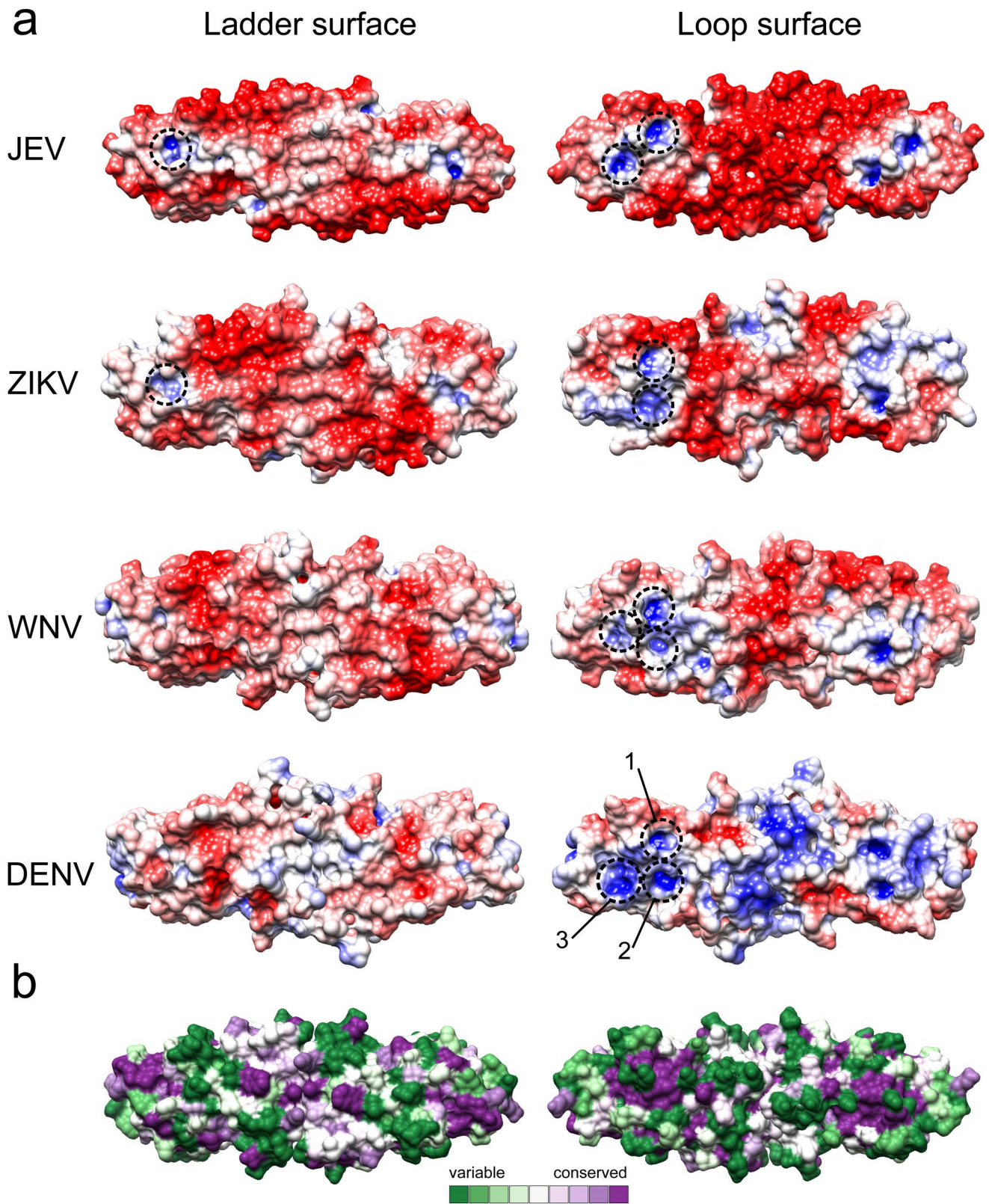
320          330          340          350
JEV_M55506   P L R F R T E N G C W Y G M E I R P V M H D E T T L V R S Q V D A
WNV_AF196835 P L R Y Q T D S G C W Y G M E I R P Q R H D E K T L V Q S Q V N A
ZIKV_KU365779.1 P L S F R A K D G C W Y G M E I R P R K E P E S N L V R S M V T A
ZIKV_AY632535 P L S F R A K D G C W Y G M E I R P R K E P E S N L V R S M V T A
DENT1_U88535  P L R F K G E D G C W Y G M E I R P V K E K E E N L V K S M V S A
DENV2_M84727  P L R Y R G E D G C W Y G M E I R P L K E K E E N L V N S L V T A
DENT3_EF643017 P L R Y M G E D G C W Y G M E I R P I S E K E E N M V K S L V S A
DENT4_AF326573 P L R F L G E D G C W Y G M E I R P L S E K E E N M V K S Q V T A
Clustal Consensus * * : . . * * * * * * * * * . * . : * * * *

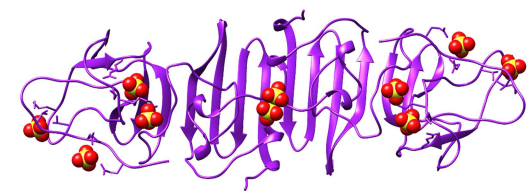
```



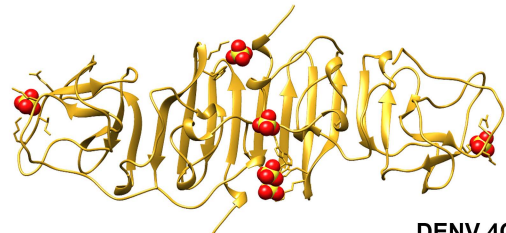




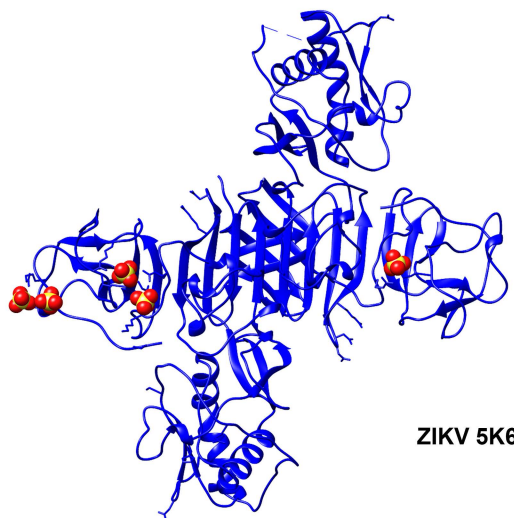




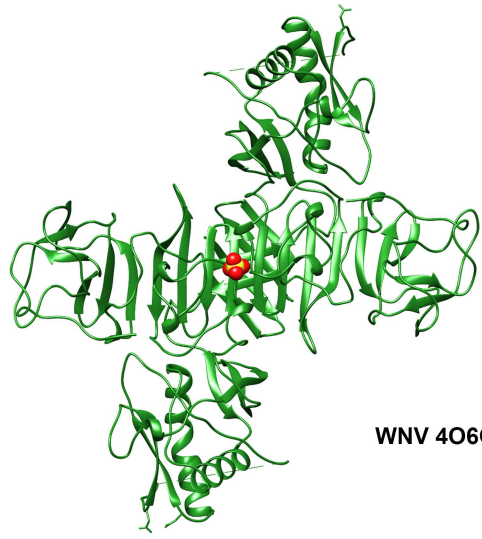
JEV



DENV 40IG



ZIKV 5K6K



WNV 406C

